

# Curvature Mapping Method: Mapping Lorentz Force in Orion A

MENGKE ZHAO <sup>1,2</sup>, GUANG-XING LI <sup>3</sup>, AND KEPING QIU <sup>1,2</sup>

<sup>1</sup>*School of Astronomy and Space Science, Nanjing University, 163 Xianlin Avenue, Nanjing 210023, Jiangsu, People's Republic of China*

<sup>2</sup>*Key Laboratory of Modern Astronomy and Astrophysics (Nanjing University), Ministry of Education, Nanjing 210023, Jiangsu, People's Republic of China*

<sup>3</sup>*South-Western Institute for Astronomy Research, Yunnan University, Kunming 650091, People's Republic of China*

## ABSTRACT

Magnetic force is a fundamental force in nature. Although widely believed to be important in counterbalancing against collapse in star formation, a clear evaluation of the role of the magnetic field in star formation remains hard to achieve. Past research attempts to evaluate the importance of magnetic forces using diagnostics such as the mass-to-flux ratio, which measures its strength but not how it functions. Since star formation is a complex process and the observed regions have complex structures, mapping the importance of the magnetic field is necessary. We propose a new technique, the Curvature Mapping Method, to evaluate the role of the magnetic force by providing maps of the magnetic force estimated using polarization observations. The Curvature Mapping Method provides maps with the contribution of the magnetic force clearly outlined. We apply the method to the star formation region of Orion A and provide a first quantitative result where the magnetic force arising from the pinched magnetic field does provide support against gravity. By comparing it against the gravitational force, we find that the magnetic force is enough to affect the low-density gas but is insufficient to support the dense region from collapse. The method effectively uses information contained in polarization maps and can be applied to data from surveys to understand the role of the B-field.

## 1. INTRODUCTION

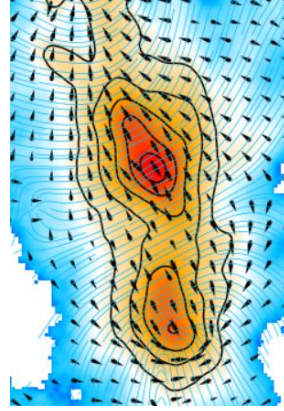
The magnetic field plays an important role in star formation (Larson 1981; McKee & Ostriker 2007; Li 2021), whose role in the star formation process is not entirely understood (Crutcher 2012; Li 2021; Pattle et al. 2023). Polarization observation (Planck Collaboration et al. 2016; Ward-Thompson et al. 2017; Harper et al. 2018) is the main magnetic field tracer, which can constrain the magnetic field morphology in the plane of the sky (POS). Large radio arrays, such as ALMA, and SKA, provide high-resolution dust polarization data to study magnetic fields of the interstellar medium (ISM) in star formation (Liu et al. 2020, 2024). The next stage is to analyze the information in these data sets to understand physics. The Davis-Chandrasekhar–Fermi (DCF; Davis 1951; Chandrasekhar & Fermi 1953) method is the most commonly used method, where the magnetic field strength is estimated through the dispersion of the polarization angle. The method is based on the assumption that the field lines are straight where the angle dispersion of the field lines is caused by turbulence, and this angle dispersion can be estimated using the dispersion of the polarization angle. However, in many cases, the magnetic field exhibits large-scale coherent structures where the assumption of almost strain fields as required in the DCF breaks down. How to analyze these data sets becomes an urgent question.

When the field lines are regular, the force is different from that is assumed in the DCF, where the field line becomes perturbed not to account for the turbulent pressure, but to counterbalance against gravity. In fact, those pinched magnetic field structures are usually interpreted as a balance between magnetic force and gravity in observations (Li et al. 2015; Pattle et al. 2017; Arzoumanian et al. 2021). Following this reasoning, Li et al. 2015 used this force balance to estimate the magnetic field strength by the balance between gravity and the Lorentz force. However Li et al. 2015 only applied this method to some particular cases, and we argue that this argument is general one can

## Curvature Mapping Method

Lorentz Force: **B-field strength** + **Curvature(feature)**

➔ **Map of Lorentz force**  $f_L \approx f_t = \frac{1}{\mu_0} B^2 \cdot \kappa$



The spatially resolved directional information is complementary to B-field strength estimated from e.g. Zeeman and DCF.

Lorentz Force (vector)  
B-field feature (line)

**Figure 1. Curvature Mapping method: mapping the Lorentz force in molecular clouds.** Lorentz force can be derived by combining magnetic field strength and the curvature of the field lines. Previous studies estimate magnetic field strength using Zeeman splitting or the DCF method. In comparison, the Curvature Mapping Method can provide spatially resolved maps of the magnetic force.

estimate the Lorentz force in a much larger variety of simulations as compared to Li et al. 2015. When data allows, one can estimate the Lorentz force at every location in the map by making use of the curvature of the polarization map, using the equation

$$f_L \approx f_t = \frac{1}{\mu_0} B^2 \cdot \kappa, \quad (1)$$

Lorentz force in ISM is close to the magnetic tension (detail shown in Ap.B), where the magnetic field curvature is derived by magnetic field morphology. Magnetic field strength  $B$  (from e.g. Zeeman or DCF method) and the magnetic field curvature  $\kappa$  (polarization) constitute the vector information of Lorentz, where the polarization provides the Lorentz force's orientation information and Zeeman provides the magnetic force's size information. Mapping the magnetic force, the Lorentz force  $f_L$ , provides a direct manner to study the effect of the magnetic field in star formation, which is another method different from the previous studies, measurement of magnetic strength (Crutcher et al. 2010; Liu et al. 2022).

## 2. LORENTZ FORCE

The Lorentz force is defined as the force acting on moving charged particles in the electromagnetic field, which is related to the magnetic field  $B$  and current density  $J$  in plasma:

$$f_L = \mathbf{J} \times \mathbf{B}, \quad (2)$$

Using Ampère's law ( $\mathbf{J} = (\nabla \times \mathbf{B})/\mu_0$ ), the Lorentz force will be measured by the magnetic field as:

$$f_L = \frac{1}{\mu_0} (\nabla \times \mathbf{B}) \times \mathbf{B} = \frac{(\mathbf{B} \cdot \nabla) \mathbf{B}}{\mu_0} - \nabla \left( \frac{B^2}{2\mu_0} \right), \quad (3)$$

where the first term is the magnetic tension and the second term is the magnetic pressure.

Assuming the distribution of magnetic field strength is uniform in ISM, the magnetic pressure could be small and not dominate the Lorentz force, in which magnetic pressure is the gradient of magnetic energy density (square of magnetic field strength, see Eq. 3). Compared with magnetic tension (see Eq. 3), magnetic tension,  $f_t$  is also easy to measure:

$$f_t = \frac{1}{\mu_0} (\mathbf{B} \cdot \nabla) \mathbf{B} = \frac{B^2}{\mu_0} (\vec{b} \cdot \nabla) \vec{b} = \frac{B^2}{\mu_0} \cdot \kappa, \quad (4)$$

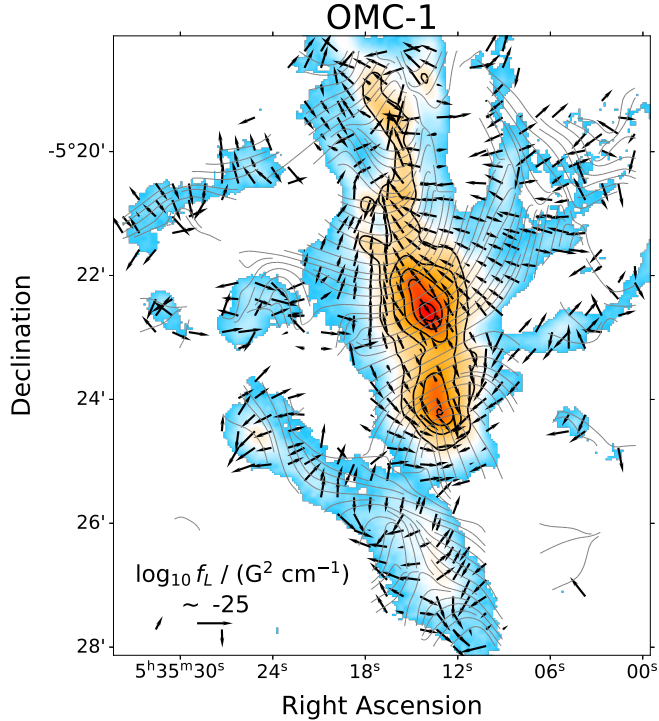


**Figure 2. Lorentz force distribution in OMC 1.** The black vectors display the Lorentz force orientation in OMC 1. The streamlines show the local magnetic field orientation. The background presents the distribution of continuum emission at the wavelength of  $850 \mu\text{m}$ . The black contours present the dense area of OMC 1.

where the  $B$  shows the magnetic field strength and  $\vec{b}$  is the unit vector of magnetic field. The  $(\vec{b} \cdot \nabla)\vec{b}$  is another parameter of the magnetic field, the curvature of the magnetic field  $\kappa$ .

Comparison between magnetic tension and Lorentz force in MHD numerical simulation with Enzo code (Collins et al. 2012; Burkhart et al. 2015), the magnetic tension resembles Lorentz force in both value and orientation (detail shown in Ap. B). Assume magnetic tension approximates Lorentz force, the Lorentz force will be estimated by magnetic tension:

$$f_L \approx f_t = \frac{1}{\mu_0} B^2 \cdot \kappa, \quad (5)$$

The magnetic field curvature is a key physical parameter, which can be derived by magnetic field orientation (polarization), and the magnetic field strength is derived by Zeeman observation (see Fig. 1). Using the advance of Zeeman observation and polarization observations, the magnetic force, Lorentz force, can be plotted as vectors in the POS (including strength and orientation of Lorentz force), which this technique is called the Curvature Mapping Method. Another advantage of the Curvature Mapping Method is that the orientation of Lorentz force is from  $0$  to  $2\pi$  although that of magnetic field derived by polarization is only  $[0, \pi]$ .

### 3. MAPPING LORENTZ FORCE IN ORION A

Orion A is a famous massive star-forming region at a distance of about 380 pc. The unique over-glass structure of the magnetic field in OMC-1 exists in this molecular cloud (see Fig. 2), which is a classic pinched magnetic field structure. Applying the Curvature Mapping Method on the magnetic field observations of OMC-1 (Falgarone et al. 2008; Pattle et al. 2017), We first plot the Lorentz force map as vectors in molecular clouds.

#### 3.1. Mapping the Lorentz Force in OMC-1

Mapping Lorentz Force in pinched magnetic field structure requires the following information: magnetic field strength (Zeeman observation) and magnetic field feature (polarization). Magnetic field strength in OMC-1 was directly measured by the Zeeman split of CN emissions (Falgarone et al. 2008):  $B = 2B_{\text{loc}} = -720 \mu\text{G}$ . The total magnetic field

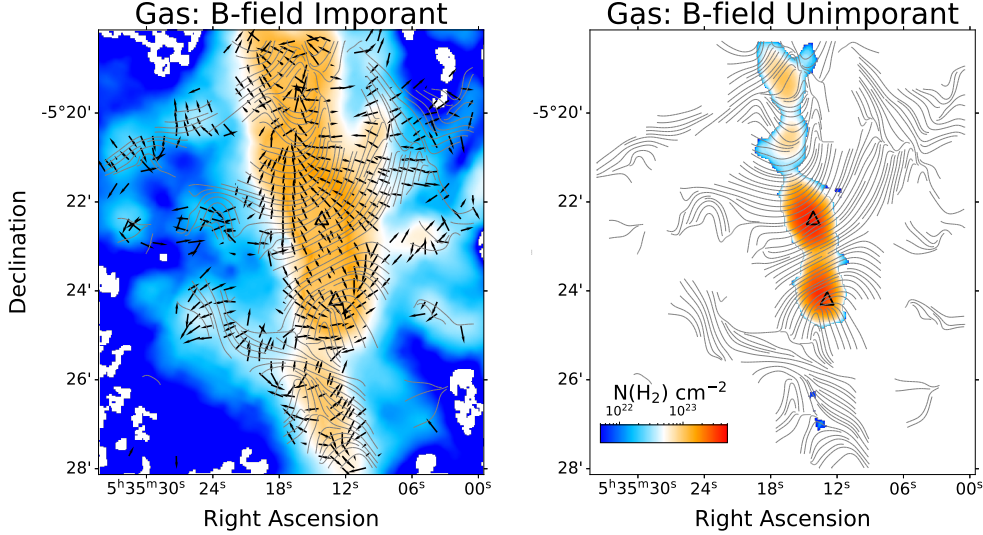


**Figure 3. Regions where can be traced by B-field observation or not.** The graphic symbol of this figure is the same as the Fig. 2. The background of panels with the same color scale shows the column density which can be traced by B-field (left panel) or not (right panel). The triangles show the position of clumps Orion-KL and Orion-S.

strength  $B$  is twice the magnetic field strength at LOS from Zeeman observation (Crutcher et al. 2010). The magnetic field orientation at POS,  $\psi_B$ , will be used to measure magnetic curvature  $\kappa$  (Eq. C4, C5, C6), which is derived by dust polarization at  $850\ \mu\text{m}$  (Ward-Thompson et al. 2017; Pattle et al. 2017).

The Lorentz force  $f_L$  in OMC-1 can be measured as:

$$f_L = \frac{1}{\mu_0} B^2 \kappa, \quad (6)$$

where the magnetic field strength  $B$  is  $-720\ \mu\text{G}$ ,  $\mu_0$  is  $4\pi$  in cgs units. We plot the vector map of Lorentz force at the plane of the sky (POS) shown in Fig. 2.

For regions with an hourglass-shaped magnetic field, the Lorentz force has a bipolar geometry that pulls towards opposition directions (see Fig. 2). The Lorentz force from this magnetic field configuration can provide some support against gravity.

### 3.2. Importance of Magnetic field

The star formation processes are derived by gas self-gravity collapse to form the newborn star (McKee & Ostriker 2007). In these physical processes, the magnetic field's importance is reflected when the B-field can balance self-gravity collapse (Arzoumanian et al. 2021; Pattle et al. 2023).

We propose magnetic critical density  $\rho_{\text{crit,B}}$ , quantity the importance of the magnetic field:

$$\rho_{\text{crit,B}} = f_L/a_G = \frac{B^2}{\mu_0} \kappa \left( \frac{G \cdot M_{\text{total}}}{r^2} \right)^{-1}, \quad (7)$$

where  $f_L$  is Lorentz force and  $a_G$  is the acceleration from gravity collapse,  $M$  is the mass of ISM and  $r$  is the equal radius of ISM. When the density of gas is below  $\rho_{\text{crit,B}}$ , the magnetic field plays an important role against self-gravity collapse. If the gas density is higher than the magnetic critical density  $\rho_{\text{crit,B}}$ , the magnetic field in this magnetic field structure will no longer be important as it cannot stop the gravitational collapse.

In the star formation region OMC-1, Orion-KL, and Orion-South are the main gravitational sources in this region, which are assumed to be one gravitational source using the equivalent sphere model (Fiege & Pudritz 2000). The total mass will be the sum of the masses of Orion-KL ( $M_1$ ) and Orion-South ( $M_2$ ), which is obtained from the column density map ( $N(\text{H}_2) > 10^{23.4}\ \text{cm}^{-2}$ ). The magnetic curvature  $\kappa$  is the mean value of OMC-1. The equivalent radius  $r$  will be  $M_2/(M_1 + M_2)$  times the distance  $L$  between Orion-KL and Orion-South. The gravitational acceleration can

be estimated as  $a_G = G \cdot M_{\text{tot}} r^{-2} = G(M_1 + M_2) \left( \frac{M_2}{M_1 + M_2} L \right)^{-2}$ . The magnetic critical density  $\rho_{\text{crit,B}}$  is around  $1.5 \times 10^5 \text{ cm}^{-3}$  in OMC-1.

To visualize the importance of the magnetic field at different locations in the cloud, we decompose the gas into two components where the role of the magnetic field is different. According to Fig. 3, the magnetic field is important in the diffuse envelope of the region. However, in the high-density regions, gravity is stronger than the magnetic force provided by the pinched magnetic field. The results imply that the magnetic field plays a limited role in the collapse.

#### 4. CONCLUSION

We propose a new technique, the Curvature Mapping Method, to plot the vector map of Lorentz force in ISM. The method is based on the idea that the Lorentz force depends on the morphology of the magnetic field, which can be traced by dust polarization. Thus, we can estimate the Lorentz force directly using dust polarization maps. The Lorentz force depends on the magnetic field strength  $B$  (Zeeman observations) and magnetic curvature  $\kappa$  (polarization observation):

$$f_L = \frac{1}{\mu_0} B^2 \cdot \kappa,$$

The magnetic force can be derived using Zeeman and polarization observations at every location in the sky.

We apply the method to observations of the massive star formation region OMC-1. By analyzing the balance between the Lorentz force and gravity, we derive magnetic critical density  $\rho_{\text{crit,B}}$

$$\rho_{\text{crit,B}} = f_L/a_G = \frac{B^2}{\mu_0} \kappa \left( \frac{G \cdot M_{\text{total}}}{r^2} \right)^{-1},$$

beyond which gravity over the magnetic field. We find that in OMC-1, the critical density is around  $1.5 \times 10^5 \text{ cm}^{-3}$ . The diffuse envelope appears magnetically dominated, and the central high-density regions are gravity-dominated.

By effectively using the information in the polarization map, the Curvature Mapping Method provides direct insights into the role of B-field in star-forming regions and can be widely applied. Compared to previous diagnostics, such as the mass-to-flux ratio, which aims to derive diagnostic measures toward whole regions, our spatially-resolved approach takes full advantage of the information in the map, leading to direction vision into the role of the magnetic field. With this unprecedented amount of polarization measurements gathered by modern instruments, by combining our results with other methods with spatial information, such as gravitational acceleration mapping (He et al. 2023), direct insights into the role of the magnetic field in regulating star formation can be obtained.

#### REFERENCES

- Arzoumanian, D., Furuya, R. S., Hasegawa, T., et al. 2021, *A&A*, 647, A78, doi: [10.1051/0004-6361/202038624](https://doi.org/10.1051/0004-6361/202038624)
- Burkhart, B., Collins, D. C., & Lazarian, A. 2015, *apj*, 808, 48, doi: [10.1088/0004-637X/808/1/48](https://doi.org/10.1088/0004-637X/808/1/48)
- Burkhart, B., Appel, S. M., Bialy, S., et al. 2020, *apj*, 905, 14, doi: [10.3847/1538-4357/abc484](https://doi.org/10.3847/1538-4357/abc484)
- Chandrasekhar, S., & Fermi, E. 1953, *ApJ*, 118, 113, doi: [10.1086/145731](https://doi.org/10.1086/145731)
- Collins, D. C., Kritsuk, A. G., Padoan, P., et al. 2012, *apj*, 750, 13, doi: [10.1088/0004-637X/750/1/13](https://doi.org/10.1088/0004-637X/750/1/13)
- Crutcher, R. M. 2012, *ARA&A*, 50, 29, doi: [10.1146/annurev-astro-081811-125514](https://doi.org/10.1146/annurev-astro-081811-125514)
- Crutcher, R. M., Wandelt, B., Heiles, C., Falgarone, E., & Troland, T. H. 2010, *apj*, 725, 466, doi: [10.1088/0004-637X/725/1/466](https://doi.org/10.1088/0004-637X/725/1/466)
- Davis, L. 1951, *Physical Review*, 81, 890, doi: [10.1103/PhysRev.81.890.2](https://doi.org/10.1103/PhysRev.81.890.2)
- Falgarone, E., Troland, T. H., Crutcher, R. M., & Paubert, G. 2008, *A&A*, 487, 247, doi: [10.1051/0004-6361:200809577](https://doi.org/10.1051/0004-6361:200809577)
- Fiege, J. D., & Pudritz, R. E. 2000, *MNRAS*, 311, 85, doi: [10.1046/j.1365-8711.2000.03066.x](https://doi.org/10.1046/j.1365-8711.2000.03066.x)
- Griffin, M. J., Abergel, A., Abreu, A., et al. 2010, *A&A*, 518, L3, doi: [10.1051/0004-6361/201014519](https://doi.org/10.1051/0004-6361/201014519)
- Harper, D. A., Runyan, M. C., Dowell, C. D., et al. 2018, *Journal of Astronomical Instrumentation*, 7, 1840008, doi: [10.1142/S2251171718400081](https://doi.org/10.1142/S2251171718400081)
- He, Z.-Z., Li, G.-X., & Burkert, A. 2023, *MNRAS*, 526, L20, doi: [10.1093/mnras/slad104](https://doi.org/10.1093/mnras/slad104)
- Larson, R. B. 1981, *MNRAS*, 194, 809, doi: [10.1093/mnras/194.4.809](https://doi.org/10.1093/mnras/194.4.809)
- Li, H.-B. 2021, *Galaxies*, 9, 41, doi: [10.3390/galaxies9020041](https://doi.org/10.3390/galaxies9020041)

- Li, H.-B., Yuen, K. H., Otto, F., et al. 2015, *Nature*, 520, 518, doi: [10.1038/nature14291](https://doi.org/10.1038/nature14291)
- Liu, J., Qiu, K., & Zhang, Q. 2022, *ApJ*, 925, 30, doi: [10.3847/1538-4357/ac3911](https://doi.org/10.3847/1538-4357/ac3911)
- Liu, J., Zhang, Q., Qiu, K., et al. 2020, *ApJ*, 895, 142, doi: [10.3847/1538-4357/ab9087](https://doi.org/10.3847/1538-4357/ab9087)
- Liu, J., Zhang, Q., Lin, Y., et al. 2024, arXiv e-prints, arXiv:2403.03437, doi: [10.48550/arXiv.2403.03437](https://doi.org/10.48550/arXiv.2403.03437)
- McKee, C. F., & Ostriker, E. C. 2007, *ARA&A*, 45, 565, doi: [10.1146/annurev.astro.45.051806.110602](https://doi.org/10.1146/annurev.astro.45.051806.110602)
- Pattle, K., Fissel, L., Tahani, M., Liu, T., & Ntormousi, E. 2023, in *Astronomical Society of the Pacific Conference Series*, Vol. 534, *Protostars and Planets VII*, ed. S. Inutsuka, Y. Aikawa, T. Muto, K. Tomida, & M. Tamura, 193, doi: [10.48550/arXiv.2203.11179](https://doi.org/10.48550/arXiv.2203.11179)
- Pattle, K., Ward-Thompson, D., Berry, D., et al. 2017, *ApJ*, 846, 122, doi: [10.3847/1538-4357/aa80e5](https://doi.org/10.3847/1538-4357/aa80e5)
- Planck Collaboration, Ade, P. A. R., Aghanim, N., et al. 2016, *A&A*, 586, A138, doi: [10.1051/0004-6361/201525896](https://doi.org/10.1051/0004-6361/201525896)
- Poglitsch, A., Waelkens, C., Geis, N., et al. 2010, *A&A*, 518, L2, doi: [10.1051/0004-6361/201014535](https://doi.org/10.1051/0004-6361/201014535)
- Polychroni, D., Schisano, E., Elia, D., et al. 2013, *apjl*, 777, L33, doi: [10.1088/2041-8205/777/2/L33](https://doi.org/10.1088/2041-8205/777/2/L33)
- Roy, A., Martin, P. G., Polychroni, D., et al. 2013, *ApJ*, 763, 55, doi: [10.1088/0004-637X/763/1/55](https://doi.org/10.1088/0004-637X/763/1/55)
- Wang, K., Testi, L., Ginsburg, A., et al. 2015, *MNRAS*, 450, 4043, doi: [10.1093/mnras/stv735](https://doi.org/10.1093/mnras/stv735)
- Ward-Thompson, D., Pattle, K., Bastien, P., et al. 2017, *ApJ*, 842, 66, doi: [10.3847/1538-4357/aa70a0](https://doi.org/10.3847/1538-4357/aa70a0)



## APPENDIX

## A. DATA

The polarized data come from the B-fields In STar-forming Region Observations (BISTRO) survey (Ward-Thompson et al. 2017; Pattle et al. 2017). The resolution of the polarization data is  $14''$  (FWHM  $\sim 0.03$  pc) measured by Scuba-2+POL-2 at  $850\mu\text{m}$ . To calculate the polarized angle, the Stokes parameters Q and U are used in the equation:

$$\psi_p = 0.5 \times \arctan(U, Q), \quad (\text{A1})$$

where polarized angle  $\psi_p$  varies from  $-90^\circ$  to  $90^\circ$ . This is the IAU convention. One has to use  $\psi = 0.5 \times \arctan(-U, Q)$  to convert Planck measurement to this IAU convention. The magnetic field (after that, B-field) orientation can be obtained by adding  $90^\circ$  to the polarized angle:  $\psi_B = \psi_p + 90^\circ$ .

The  $\text{H}_2$  column density map in the molecular cloud, OMC-1, comes from Herschel Gould Belt Survey<sup>1</sup> (Poglitsch et al. 2010; Griffin et al. 2010; Roy et al. 2013; Polychroni et al. 2013), which apply the SED fitting procedure (Wang et al. 2015) on the Herschel continuum at wavelengths of 70, 160, 250, 350,  $500\mu\text{m}$ .

## B. LORENTZ FORCE AND MAGNETIC TENSION IN ENZO SIMULATION

For this study, we identified a molecular cloud through self-gravitating simulations using the constrained transport MHD option in Enzo (MHDCT) code (Collins et al. 2012; Burkhart et al. 2015, 2020). The simulations aimed to analyze the effects of self-gravity and magnetic fields on supersonic turbulence in iso-thermal molecular clouds. We use the simulation data ( $\beta = 20$ ,  $t \approx 0.76$  Myr). This simulation setup is chosen such that the results resemble the structure of an actual star-forming molecular cloud. The Lorentz force and magnetic tension are measured in 3D space as Eq. 3 and Eq. 4. With the density increasing, Lorentz force stays at a similar value with the magnetic tension (See Fig. 4). The Lorentz force is comparable to the magnetic tension.

We compare the Lorentz, force, magnetic tension, magnetic pressure in 3D space (Collins et al. 2012; Burkhart et al. 2015, 2020), where the similarity of two vectors, magnetic tension and Lorentz force, is defined as:

$$D_{\text{similarity}} = \frac{\vec{v}_1 - \vec{v}_2}{\vec{v}_1 + \vec{v}_2} = \frac{f_L - f_t}{f_L + f_t} \approx \theta_{\text{offset}} \quad (\text{B2})$$

The similarity is close to the offset angle between two vectors, magnetic tension, and Lorentz force, in geometry (see Fig. 1). The similarity and offset angle in the 2D plane (POS) will be needed in actual observation. The offset angle in 3D space has a different probability density (see Ap. D). To obtain the accuracy offset angle, the distribution of the offset angle is weighted by the probability density function (see Ap. D). The offset angle between magnetic tension and Lorentz force in the 2D plane (similar to the POS) is around  $11^\circ$  and they have similar sizes (see Fig. 5). The magnetic tension resembles the Lorentz force in both magnitude and orientation.

## C. METHOD: MAPPING LORENTZ FORCE

The magnetic field orientation  $\phi_B$  in POS, measured by dust polarization, distributes from 0 to  $\pi$ . The unit vector of magnetic field  $\vec{b}$  can be decomposition by magnetic field orientation  $\psi_B$ :

$$\vec{b} = \cos\psi_B \mathbf{i} + \sin\psi_B \mathbf{j}, \quad (\text{C3})$$

where  $\mathbf{i}$  and  $\mathbf{j}$  are the unit vector of x-axis and y-axis. Measuring magnetic curvature  $\kappa$  will be possible:

$$\kappa_x = \cos\psi_B \frac{\partial}{\partial x} \cos\psi_B + \sin\psi_B \frac{\partial}{\partial y} \cos\psi_B, \quad (\text{C4})$$

$$\kappa_y = \cos\psi_B \frac{\partial}{\partial x} \sin\psi_B + \sin\psi_B \frac{\partial}{\partial y} \sin\psi_B, \quad (\text{C5})$$

<sup>1</sup> [http://www.herschel.fr/cea/gouldbelt/en/Phocaea/Vie\\_des\\_labos/Ast/ast\\_visu.php?id\\_ast=66](http://www.herschel.fr/cea/gouldbelt/en/Phocaea/Vie_des_labos/Ast/ast_visu.php?id_ast=66)

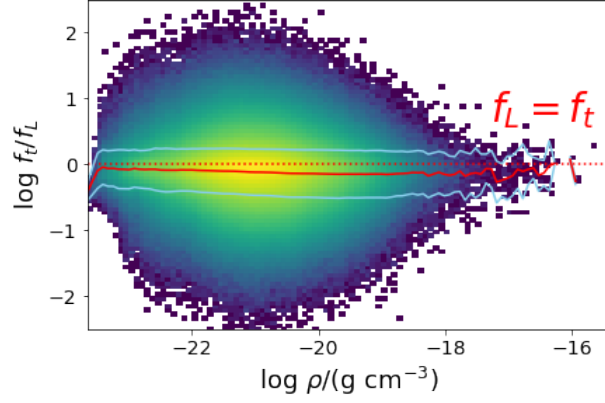


**Figure 4. Distribution of the ratio between Lorentz Force and Magnetic Tension in Enzo simulations.** The red line presents the mean value of the ratio between Lorentz Force and magnetic tension at each density range and the blue lines show the dispersion. The red dot line shows the  $f_L/f_L = 1$ .

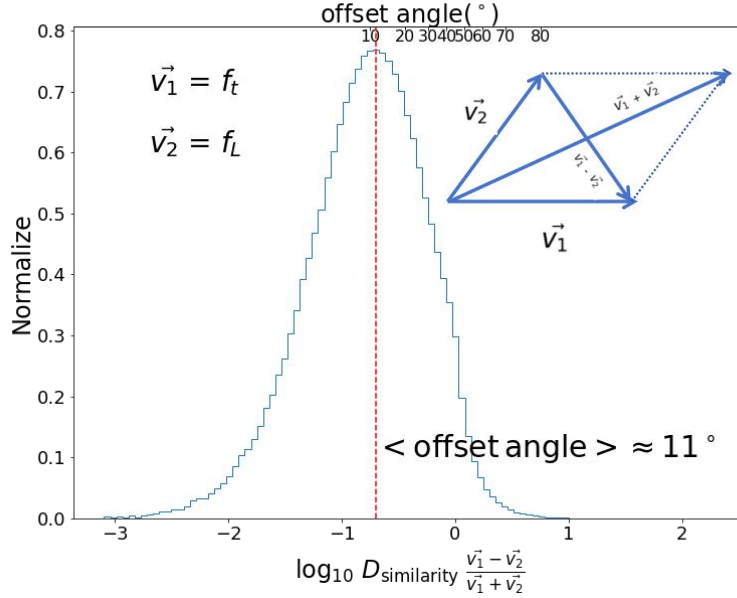


**Figure 5. Distribution of similarity and offset angle between Lorentz force and magnetic tension.** By projecting from 3D space to the 2D plane, magnetic tension  $\vec{V}_1$  is close to Lorentz force  $\vec{V}_2$ , whose offset angle is around  $11^\circ$ . The canton in the top right corner displays the similarity of two vectors.

$$\boldsymbol{\kappa} = \kappa_x \mathbf{i} + \kappa_y \mathbf{j}, \quad (\text{C6})$$

where the  $\kappa_x$  and  $\kappa_y$  are the components of curvature  $\kappa$  at x-axis and y-axis. Using the curvature  $\kappa$  (polarization components) and strength  $B$  of the magnetic field (Zeeman observations), the magnetic force, Lorentz  $f_L$ , will be measured as:

$$f_L \approx \frac{B^2}{\mu_0} \cdot \boldsymbol{\kappa}, \quad (\text{C7})$$

#### D. REMOVE THE PROJECTION EFFECT IN PROBABILITY DENSITY DISTRIBUTIONS

The probability density function,  $p(\theta)$ , of the angle between two vectors of random distribution is distributed in an  $N$ -dimensional space as:

$$p(\theta) = \frac{\Gamma(\frac{n}{2})}{\Gamma(\frac{n-1}{2})} \frac{\sin^{n-2}(\theta)}{\sqrt{\pi}} \quad (\text{D8})$$

where  $n$  is the number of dimensions, and  $\theta$  is the angle between two vectors of random distribution.



In 3-dimension space, the probability density function of angle  $p(\theta)$  is

$$p(\theta) = \frac{1}{2} \sin\theta \quad (\text{D9})$$

To remove the projection effect, we use the probability density function  $p(\theta)$  to weight the angle distribution:

$$P(\theta_{\text{corrected}}) = P(\theta_{\text{original}})/p(\theta) \quad (\text{D10})$$

where  $\theta_{\text{original}}$  represents the original angle distribution and  $\theta_{\text{corrected}}$  represents the corrected angle distribution, with the projected effects removed.